Initial Structure and Growth Dynamics of $YBa_2Cu_3O_{7-\delta}$ during Pulsed Laser Deposition

V. Vonk,[1,2,*] K. J. I. Driessen,[2] M. Huijben,[1,†] G. Rijnders,[1] D. H. A. Blank,[1] H. Rogalla,[1] S. Harkema,[1] and H. Graafsma[2,‡]

[1]*Faculty of Science and Technology,* MESA+ *Research Institute, University of Twente, P.O. Box 217, 7500 AE Enschede, The Netherlands*

[2]*European Synchrotron Radiation Facility, 6 rue Jules Horowitz, 38043 Grenoble, France*

(Received 8 March 2007; published 9 November 2007)

The initial heteroepitaxial growth of $YBa_2Cu_3O_{7-\delta}$ films on $SrTiO_3(001)$ substrates during pulsed laser deposition shows a growth-mode transition and a change of growth unit. The growth starts with two blocks, each two-thirds the size of the complete unit cell. The first of these blocks grows in a step-flow fashion, whereas the second grows in the layer-by-layer mode. Subsequent deposition occurs layer-by-layer of complete unit cells. These results suggest that the surface diffusion in the heteroepitaxial case is strongly influenced by the competition with formation energies, which is important for the fabrication of heteroepitaxial devices on the unit cell scale.

DOI: 10.1103/PhysRevLett.99.196106 PACS numbers: 68.55.Ac, 61.10.−i, 68.35.−p, 81.15.Fg

Nanoscale structures are undoubtedly a major aspect of contemporary materials science. By attempting to control the shape, crystallinity, and defects of structures at the atomic level, the limits of performance, characterization, and theoretical knowledge are challenged. The high-T_c superconductor $YBa_2Cu_3O_{7-\delta}$ (YBCO) is a good example of the aforementioned issues. In thin film form, it can be integrated in devices used in electronics, biophysics, and magnetic and x-ray sensors [1]. By nanostructuring of thin films of YBCO it is possible to study the symmetry of the superconducting order parameter, thereby giving fundamental insights into high-T_c superconductivity [2].

Pulsed laser deposition (PLD) is a technique well suited for the fabrication of thin perovskitelike films. The dynamics of the growth during PLD have been extensively studied using reflection high energy electron diffraction (RHEED) [3,4]. However, with RHEED it is not possible to obtain detailed information about the atomic structure during growth, which motivated the use of x rays [5–11]. Here we report on x-ray diffraction measurements during the PLD growth of YBCO on $SrTiO_3(001)$ (STO).

The experiments were carried out using a specially designed PLD chamber [12] at the European Synchrotron Radiation Facility on BM26 (DUBBLE) [13], using an x-ray wavelength of 0.775(1) Å. A KrF excimer laser beam (wavelength $\lambda = 248$ nm) was focused on the sintered YBCO target, resulting in a laser fluence of approximately 1.5 $J\,cm^{-2}$. During deposition the TiO_2-terminated [14] substrate temperature was kept at 1053 K, while the oxygen pressure was 0.1 mbar. Five TiO_2-terminated substrates, labeled I through V hereafter and differing only in their miscut angles, were used in the measurements.

In order to extract the structure evolution of the film during deposition, a distributed growth model [15] is used. The coverage θ of the jth layer is evaluated as a function of time by solving the following set of coupled differential equations:

$$\frac{d\theta_j}{dt} = (1 - \lambda_{j-1})\frac{1}{\tau}(\theta_{j-1} - \theta_j) + \lambda_j \frac{1}{\tau}(\theta_j - \theta_{j+1}) \quad (1)$$

with τ the time needed to deposit a complete monolayer. The interlayer mass transport, λ, is made coverage-dependent by using the following relation [16]:

$$\lambda_j = 1 - \exp\left(\frac{-\alpha\sqrt{\frac{1}{2} - |\theta_{j-1} - \frac{1}{2}|}}{\theta_{j-1}}\right) \quad (2)$$

with α a dimensionless parameter. When $\alpha \to \infty$, there is perfect layer-by-layer or step-flow growth [17]; for each layer $\lambda_j = 1$, which means that all the material that arrives at a certain level will diffuse to the level below. The other extreme case, $\alpha = 0$, results in Poisson growth. The difference with the model of Ref. [16] is that here the term accounting for a gradual decrease of interlayer mass transport is omitted.

The results of monitoring the $(0, 0, 0.175)$ reciprocal space point in STO units [18] during deposition of sample I are shown in Fig. 1(a). The oscillating intensity indicates that the surface cycles between smooth and rough morphologies. However, the time that elapses between the consecutive intensity maxima is not constant. The two very first smooth layers (B and C) are each deposited in 2/3 of the time of the following unit cell layers. Furthermore, the intensity increases upon starting the deposition. In order to understand these features in detail, the previously described coverages of each layer are used to calculate the scattered intensity by

$$I(l, t) = \begin{cases} I_{\mathrm{SF}}(l, \theta_j(t)) + I_{\mathrm{bg}}, & \text{for } j = 0, \\ I_{\mathrm{LBL}}(l, \theta_j(t)) + I_{\mathrm{bg}}, & \text{for } j \geq 1, \end{cases} \quad (3)$$

where l is the reciprocal space point in reciprocal lattice units (r.l.u.), I_{bg} is a constant x-ray background, and I_{SF} and I_{LBL} give the intensities expected for step-flow (SF) and layer-by-layer (LBL) growth by

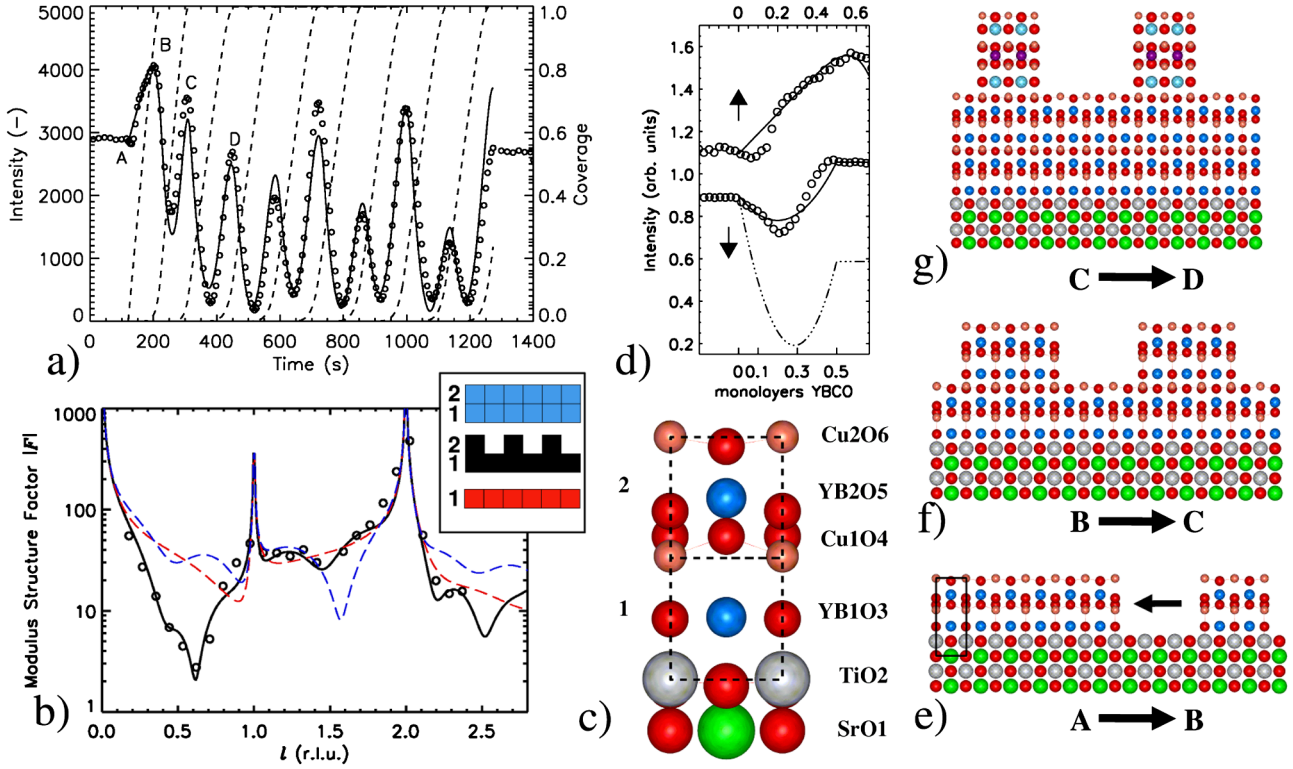

FIG. 1 (color online). Experimental data obtained from the diffraction measurements and the resulting real space images. For the latter the following color/size-gray scale coding is used: Ti (gray/large-bright), O (red/small-dark), Sr (green/large-midtone), Cu (light red/small-bright), YB (blue/small-dark), Y (purple/small-dark), and Ba (light blue/large-bright). The oxygens with site occupancies of 1 and 2/3 are distinguished by the former being slightly larger. (a) The intensity growth oscillations (open circles) and the model fit (solid line) described by Eq. (3). Deposition started at point A (120 s). The coverage of each layer as a function of time (dashed line) follows from Eqs. (1) and (2). (b) The specular CTR of sample III at deposition conditions after growth of half a monolayer YBCO. Open circles indicate measured data points and the solid line is the fit. The inset schematically shows three different morphologies, which would be expected for nominal coverages of 1/3 (red, bottom), 1/2 (black, middle, best fit), and 2/3 (blue, top). The corresponding CTR's are presented with the date for 1/3 (red, dashed line), 1/2 (black, solid line), and 2/3 (blue, dashed line). (c) The structure of the half monolayer YBCO of sample III that results from fitting the specular CTR shown in (b). The resulting interatomic distances are listed in Table II. (d) The experimental data (open circles) of the very first intensity oscillation for samples I (upper, miscut $\xi = 0.38^{\circ}$) and III (lower, miscut $\xi = 0.06^{\circ}$) and the fits (solid line) as described in the text. Also shown is the expected intensity oscillation for sample III (dashed line) when assuming complete LBL growth ($\beta = 0$). (e)–(g) The structure at different stages A through D [as indicated in (a)] of the growth during deposition. A to B: the initial step-flow growth of a block as indicated by the rectangle, which is shown enlarged in (c). B to C: formation of two-dimensional islands with an atomic structure as in (c). C to D: formation of two-dimensional islands with the bulk YBCO atomic structure.

$$I_{\mathrm{SF}} = s\{[1-\theta_j(t)]|F_{\mathrm{CTR}}(l)|^2 + \theta_j(t)|F_{\mathrm{CTR}}(l)+F_0|^2\},$$
$$I_{\mathrm{LBL}} = s\left|F_{\mathrm{CTR}}(l)+F_0+\theta_1(t)F_0 e^{i2\pi l} + \sum_{j=2}^{n}\theta_j(t)F_{\mathrm{ybco}}(l)e^{i2\pi l\Delta z}e^{i2\pi lj}\right|^2, \quad (4)$$

where s is a scale factor, F_{CTR} is the crystal truncation rod (CTR) scattering of the substrate [19], F_0 describes the scattering from each of the two first layers, F_{ybco} is the structure factor of a complete YBCO unit cell taken from the bulk structure [20], and Δz is the displacement of the complete unit cell layers YBCO with respect to the layers underneath. For the complete film, a c axis of 11.91(5) Å has been measured, corresponding to the YBCO bulk value at 1053 K. Furthermore, the very first layer is assumed to grow in a SF fashion, which requires one to consider the sum of the resulting *intensities* of the covered and uncovered substrates as a function of time. From the second layer onward, growth proceeds in the LBL mode. This finding will be discussed in more detail later on. The results of fitting Eq. (3) to the data are listed in Table I and shown in Fig. 1(a).

In order to understand the structure, and thereby F_0, of an ultrathin YBCO film, the specular CTR of sample III was measured after deposition of half a unit cell layer. The data [see Fig. 1(b)] were integrated, corrected, and used in a refinement procedure using the ANA-ROD package [21].

The structural model that fits the data best emerges from the following assumptions and restraints, which were derived from previously published results on the growth and (surface) structure of YBCO and related materials. The

TABLE I. Results obtained from fitting the model as described in the text to the intensity growth oscillations of Fig. 1(a). The listed parameters are given by Eqs. (3) and (4).

Parameter	Value	Parameter	Value
s	0.46(7)	τ(s)	137.7(2)
$\lvert F_0\rvert$	159(1)	l (r.l.u.)	0.175
ϕ_0 (rad)	1.34(8)	I_{bg} (counts)	100
α	3.7(3)	Δz	0.15

model consists of perovskitelike blocks ABX_3, with $A = Y_{1/3}Ba_{2/3}$, $B = Cu$, and $X = O_{2/3}$. These represent the average structure in the case that the Y and Ba atoms would not be ordered in the bulk YBCO structure. The stoichiometry is fixed in the refinement procedure, where the best fit is obtained when half of the oxygen atoms are missing in the surface copper-oxide planes [Cu2-O6 and half of the Cu1-O4 plane] [22]. The atomic stacking across the interface is assumed to continue the network of oxygen octahedra, with Ti at their centers in the substrate and Cu in the film. Starting values for the atomic positions in the refinement were derived from the bulk structures $LaYBa_2Cu_2Ti_2O_{11}$ [23] and YBCO [20]. The results are listed in Table II, and a schematic picture of the structure is shown in Fig. 1(c).

The best fit model consists of two layers of the ABX_3 blocks, denoted 1 and 2 in Fig. 1(c). The layer at the interface (1) is fully covering the substrate and the one on top (2) is covering half of the surface. Such a morphology would give rise to step-heights on the surface of about 4 and possibly 8 Å, which is in good agreement with previous studies on ultrathin RBCO films, with $R = Y$ [24], Sm [25]. Test models having different morphologies are clearly distinguished as shown in Fig. 1(b). This result suggests that in the case of sample III the nucleation proceeds differently compared to sample I, which is, as discussed later on, due to the different miscut angles of the substrates. However, using the structural model to calculate the structure factor in the case of fully occupied layers 1 and 2 at point $l = 0.175$ results in $|F_0^*| = 159$ and $\phi_0^* = 1.64$. This agrees rather well with the results obtained for F_0 shown in Table I and suggests strongly that the growth unit during initial deposition of sample I resembles the presented structural model very much.

TABLE II. Interatomic distances in the z direction and the rumpling in the different planes obtained from fitting the specular CTR at 1053 K. Notation is taken as in Fig. 1(c), with YB = $Y_{1/3}Ba_{2/3}$. For comparison, $a_{sto} = 3.935$ Å at 1053 K.

Atoms	Distance (Å)	Plane	Rumpling (Å)
Ti-Cu1	4.27(3)	Ti-O2	−0.2(1)
Cu1-Cu2	4.23(4)	YB1-O3	0.0(1)
Sr-YB1	3.93(1)	Cu1-O4	+0.7(1)
YB1-YB2	4.18(3)	YB2-O5	−0.7(3)
$(Sr\text{-}Ti)_z$	1.77(2)	Cu2-O6	−0.4(3)

It was not possible to obtain a more extensive data set, since about 1 h after deposition the ultrathin film was found to be unstable. A possible mechanism for the deterioration of the structure is that the copper-oxide planes at the surface are slowly reduced. The oxygen leaves the surface at defects that are reached by in-plane diffusion. When the total oxygen content drops below a critical value, the structure becomes unstable and a, so far unidentified, new phase is formed. It must be emphasized that the current method and data do not allow one to determine and refine all the details of the oxygen content, of which the uncertainty is estimated to be somewhere between 0.5 and 1 oxygen atom. Nevertheless, the perovskitelike model structure provides a framework of heavier elements, which allows it to be refined and which consistently explains all the observations.

Unlike room temperature experimental results for thicker films [26], our best fit model shows that the A site is randomly occupied by Ba and Y. This finding is further supported by all the tried test models (including ordering of Y and Ba over the A sites) resulting in approximately equal Ti-Cu1 and Cu1-Cu2 distances. In case of A site ordering this would not be expected, since an $YCuO_y$ block is considerably smaller than a $BaCuO_x$ block, 3.42 and 4.18 Å, respectively. The mechanism could be such that with increasing thickness the A site orders, simply because there is enough material. The ordering then leads to different interfacial stacking sequences substrate-TiO_2-$BaCuO_x$-$BaCuO_x$-$YCuO_y$-... and substrate-TiO_2-$BaCuO_x$-$YCuO_y$-$BaCuO_x$-... [24,26], thereby forming commonly observed antiphase boundaries [26] and possibly leading to different surface terminations [22].

Figure 1(d) shows different shapes for the first intensity oscillation of samples I and III. For sample I the intensity increases linearly, whereas for sample III it decreases parabolically. These differences indicate SF (sample I) and LBL (sample III) growth. In the former case there is no roughening of the surface and the scattering is given by the sum of intensities of the covered and the uncovered substrates. The latter situation implies nucleation of two-

TABLE III. Results for the obtained initial growth modes for all samples. The average terrace width L_s results from the miscut angle ξ. In all experiments, the substrate temperature was 1053 K. The intensity at point $l = 0.175$ increasing (+) or decreasing (−) upon deposition start is a consequence of different growth modes (SF-LBL). The parameter β describes the fraction of material nucleating by SF.

Sample	ξ (deg)	L_s (nm)	Intensity	β	Mode
I	0.38(5)	60	+	1.00	SF
II	0.22(8)	100	+	1.00	SF
III	0.06(5)	370	−	0.65	LBL/SF
IV	0.12(5)	190	−	0.80	LBL/SF
V	0.10(5)	220	−	0.70	LBL/SF

dimensional islands on the terraces. The resulting scattering arises from a mixed contribution on the scale of the x-ray coherence length [19] of the bare and covered substrates. This leads to the inequality $|F_{\mathrm{CTR}} + \epsilon F_0|^2 < |F_{\mathrm{CTR}}|^2 < (1-\epsilon)|F_{\mathrm{CTR}}|^2 + \epsilon|F_{\mathrm{CTR}} + F_0|^2$, where ϵ is an arbitrary number with $0 < \epsilon < 1$, showing that the intensity expected from SF is higher. Since simultaneous nucleation on the terraces and at the step-edges is conceivable, a parameter β is defined determining the fraction of material nucleating by step-flow. The scattered intensity is then given by $I_{\mathrm{tot}} = \beta I_{\mathrm{SF}} + (1-\beta) I_{\mathrm{LBL}}$, with I_{SF} and I_{LBL} as in Eq. (4). Figure 1(d) shows simulations for the very first intensity oscillation of sample III for $\beta = 0.65$ and 0.00.

The results for sample I lead to the conclusion that the diffusion length changes *during* growth. In order to estimate the initial diffusion length, $l_{d,\mathrm{init}}$, experiments have been carried out on five TiO_2-terminated substrates, having different miscut angles with respect to the [001] direction. The results, listed in Table III, show a clear correlation between the miscut angle and the scattered intensity increasing or decreasing upon starting the deposition.

The present results indicate that the diffusion length of the very first layer is around 150 nm, much larger than reported values for YBCO growth ranging from 7 to 22 nm [27,28]. A rough estimate of the difference in the activation energy can be obtained from the diffusion relation by $\Delta E = \ln(l_d/l_{d,\mathrm{init}}) \times 2k_B T = -0.4(1)$ eV [29]. This would represent a substantial part of the activation barrier for diffusion being around 1 eV for complex oxide growth at about 1000 K [30]. An explanation might be that when the terminating atomic layer changes from STO to YBCO, the energy landscape for diffusion changes. Furthermore, with initial nucleation taking place only at the substrate steps (SF), the additional energy barrier for diffusion over the step, the so-called Ehrlich-Schwöbel barrier can change. This may result in it being easier for adatoms to ascend a step instead of descend [31]. Indeed, a scanning tunneling microscopy study of ultrathin YBCO films has revealed that nucleation occurs preferentially at the upper step [24], quite different from homoepitaxy.

In the case of heteroepitaxial deposition of $SrRuO_3$ (SRO) on STO(001), a change in growth mode during initial nucleation has been observed as well [32]. However, in that case growth started as LBL and changed to SF. Interestingly, the lattice mismatch between SRO and STO leads to compressive strain in the film, opposite to the present system. Compressive strain has been found to lower the activation barrier for surface diffusion [33], opposite from tensile strain, and is therefore another important parameter in heteroepitaxial growth.

In conclusion, the change from one atomic structure to another involves dramatic changes in the surface free energies, thereby altering the growth completely. In the case of YBCO growth on STO(001) both the growth unit and the growth mode change during the course of the nucleation of the two first layers. These results are very important in view of the fabrication of real heteroepitaxial devices on the unit cell scale.

The authors thank B. Gorges, L. Barthe, and the staff of DUBBLE@ESRF for technical assistance during the measurements and A. Stierle and H. Dosch for fruitful discussions. The Netherlands Organization for Scientific Research (NWO) is acknowledged for financial support.

*vonk@mf.mpg.de
Present address: Max-Planck-Institute for Metals Research, Heisenbergstrasse 3, D-70765 Stuttgart, Germany.
†Present address: Department of Physics, University of California, Berkeley, CA, USA.
‡Present address: DESY, Notkestrasse 85, D-22607 Hamburg, Germany.

[1] *Thin Films and Heterostructures for Oxide Electronics*, edited by S. B. Ogale (Springer Science and Business Media, New York, 2005).
[2] J. R. Kirtley *et al.*, Nature Phys. **2**, 190 (2006).
[3] H. Karl and B. Stritzker, Phys. Rev. Lett. **69**, 2939 (1992).
[4] A. J. H. M. Rijnders *et al.*, Appl. Phys. Lett. **70**, 1888 (1997).
[5] G. Eres *et al.*, Appl. Phys. Lett. **80**, 3379 (2002).
[6] H.-H. Wang *et al.*, J. Appl. Phys. **96**, 5324 (2004).
[7] A. Fleet *et al.*, Phys. Rev. Lett. **94**, 036102 (2005).
[8] A. Fleet *et al.*, Phys. Rev. Lett. **96**, 055508 (2006).
[9] P. R. Willmott *et al.*, Phys. Rev. Lett. **96**, 176102 (2006).
[10] J. Z. Tischler *et al.*, Phys. Rev. Lett. **96**, 226104 (2006).
[11] V. Vonk *et al.*, Phys. Rev. B **75**, 235417 (2007).
[12] V. Vonk *et al.*, J. Synchrotron Radiat. **12**, 833 (2005).
[13] M. Borsboom *et al.*, J. Synchrotron Radiat. **5**, 518 (1998).
[14] G. Koster *et al.*, Mater. Sci. Eng. B **56**, 209 (1998).
[15] P. I. Cohen *et al.*, Surf. Sci. **216**, 222 (1989).
[16] H. A. van der Vegt *et al.*, Phys. Rev. Lett. **68**, 3335 (1992).
[17] Within this model, it does not contain any information about the island-size distribution. Merely the interlayer mass transport is described. Therefore within this model step-flow and perfect layer-by-layer are indistinguishable.
[18] This is very close to the ''anti-Bragg'' position of bulk YBCO.
[19] I. K. Robinson, Phys. Rev. B **33**, 3830 (1986).
[20] T. Lippmann *et al.*, Acta Crystallogr. Sect. A **59**, 437 (2003).
[21] E. Vlieg, J. Appl. Crystallogr. **33**, 401 (2000).
[22] X. Torrelles *et al.*, Phys. Rev. B **70**, 104519 (2004).
[23] K. B. Greenwood *et al.*, Chem. Mater. **7**, 1355 (1995).
[24] T. Haage *et al.*, Phys. Rev. Lett. **80**, 4225 (1998).
[25] V. C. Matijasevic *et al.*, Phys. Rev. Lett. **76**, 4765 (1996).
[26] S. Bals *et al.*, Physica (Amsterdam) **355C**, 225 (2001).
[27] T. Haage *et al.*, Surf. Sci. **370**, L158 (1997).
[28] T. Wang *et al.*, Supercond. Sci. Technol. **15**, 1199 (2002).
[29] The error represents the scatter of the different literature values.
[30] P. R. Willmott, Prog. Surf. Sci. **76**, 163 (2004).
[31] I. Markov, Phys. Rev. B **50**, 11271 (1994).
[32] G. Rijnders *et al.*, Appl. Phys. Lett. **84**, 505 (2004).
[33] M. Schroeder and D. E. Wolf, Surf. Sci. **375**, 129 (1997).